Soft Matter

Capillary Bridge Rupture in Dip-Pen Nanolithography

Journal:	*Soft Matter*
Manuscript ID:	SM-ART-05-2014-000997.R1
Article Type:	Paper
Date Submitted by the Author:	10-Jun-2014
Complete List of Authors:	Mirkin, Chad; Northwestern University, Department of Chemistry Eichelsdoerfer, Daniel; Northwestern University, Chemistry Brown, Keith; Northwestern University, Department of Chemistry

TOC GRAPHIC:

When fluid is transferred onto a surface from a nanoscale tip, the contact angle determines the character and dynamics of the fluid flow.

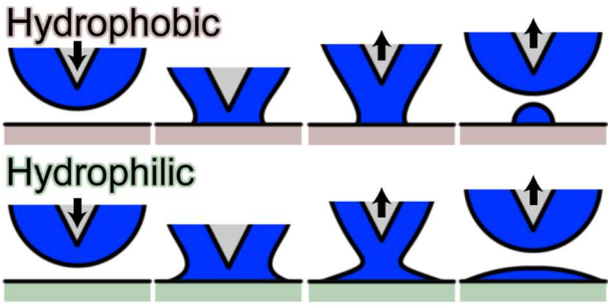

Capillary Bridge Rupture in Dip-Pen Nanolithography

*Daniel J. Eichelsdoerfer[1,†], Keith A. Brown[1,2,†], and Chad A. Mirkin[1,2,]**

[1]Department of Chemistry, [2]International Institute for Nanotechnology, Northwestern University, 2145 Sheridan Road, Evanston, IL 60208

[†]These authors contributed equally.

*To whom correspondence should be addressed. E-mail: chadnano@northwestern.edu.

Here, we explore fluid transfer from a nanoscale tip to a surface and elucidate the role of fluid flows in dip-pen nanolithography (DPN) of liquid inks. We find that while fluid transfer in this context is affected by dwell time and tip retraction speed from the substrate, their specific roles are dictated by the contact angle of the ink on the surface. This is shown by two observations: (1) the power law scaling of transferred fluid with dwell time depends on contact angle, and (2) slower retraction speeds result in more transfer on hydrophilic surfaces, but *less* transfer on hydrophobic surfaces. These trends, coupled with the observation of a transition from quasi-static to dynamic capillary rupture at a capillary number of 6×10^{-6}, show that the transfer process is a competition between surface energy and viscosity. Based on this, we introduce retraction speed as an important parameter in DPN and show that it is possible to print polymer features as small as 14 nm. Further explorations of this kind may provide a useful platform for studying capillary phenomena at the nanoscale.

INTRODUCTION

Nanoscale fluid flows govern several important processes[1] including hydraulic fracturing, molecular transport in cells, and dip-pen nanolithography (DPN)[2-5], or the controlled printing of materials using an atomic force microscope (AFM) probe coated with a solution of molecules. Fluidic effects in DPN are particularly important when considering the deposition of liquids, including certain polymers and non-volatile fluids[5-10]. While the transfer process that governs DPN of liquids is complex, it has been recognized that capillarity[11], viscosity[9], and surface

energy[6, 11] play major roles. In spite of this recent attention, many contradicting reports exist in the literature regarding the rate at which material transfer occurs[6-10] and no unifying model has been presented. This lack of understanding is particularly striking given that the importance of capillary forces in AFM imaging has motivated many theoretical and experimental studies of tip-sample forces from capillary condensation[12-15] and contact with fluid-coated surfaces[16, 17].

To understand the important factors in DPN of liquids, it is useful to separate the process into stages (Fig. 1): (i) the tip approaching and coming into contact with the surface, (ii) the tip remaining in static contact for a specified dwell time t, (iii) the tip moving away from the surface, and (iv) the breaking of the capillary bridge. The DPN literature has focused exclusively on step (ii), due in part to the success of a point diffusion model in describing the behavior of small molecules being transported from a tip to a surface[5, 18]. Despite its questionable applicability to inks other than small molecules, this heuristic has been broadly applied to all ink-sample systems, including liquid inks[19], dendrimers[20], oligonucleotides[21], and conductive polymers[22]. It seems reasonable that the deposition of inks that behave like fluids may be better understood by drawing from the large body of work in the fluid dynamics community on capillary rupture (steps iii and iv), which shows that fluid transfer between two surfaces is governed by contact angle differences and retraction speed[11, 23-26]. Such processes are commonly parameterized by the dimensionless capillary number $Ca = \mu U/\gamma$, where U is the retraction speed, μ is the dynamic viscosity, and γ is surface tension. Based on this understanding, we hypothesize that the DPN of liquids is governed by capillarity and thus should be strongly influenced by retraction speed and dwell time.

In this paper, we explore the importance of capillarity in DPN by examining the transfer of an aqueous solution of poly(ethylene glycol) (PEG) from an AFM tip to a surface. The

transfer process was studied using AFM-based force-distance analysis and by imaging the deposited material. First, we find that retraction velocity (step iii) plays a major role and observe a transition in capillary rupture (step iv) from a quasi-static regime to a dynamic retraction regime at a critical *Ca* commensurate with what is seen in flows in porous materials. Interestingly, the nature of this transition is highly dependent on surface energy, with faster retraction speeds resulting in smaller features on hydrophilic surfaces and larger features on hydrophobic surfaces. Furthermore, we find that the dependence of deposited material volume *V* on *t* (step ii) is highly dependent on surface energy, with deposition onto hydrophilic surfaces proceeding akin to capillary action and deposition onto hydrophobic surfaces proceeding more slowly, commensurate with droplet spreading behavior. We also observe that while the aspect ratio of the domed polymer features present after deposition correlates with the macroscopic contact angle, quantitative agreement is achieved by including a contribution due to the polymer-air-surface line tension. Finally, this understanding is used to pattern polymer features as small as 14 nm. In addition to this advance in lithographic capabilities, these studies highlight the rich phenomenology present in DPN and the benefits that can be garnered through a more detailed understanding of nanoscale fluid processes.

EXPERIMENTAL

In a typical force-distance experiment, a contact mode AFM probe (CONTR, spring constant ~ 0.2 N/m, NanoWorld) that had been plasma-cleaned in air (20W for 30s at 200 mTorr), then coated with an aqueous solution of 0.5 wt% PEG2000 (hereafter PEG; Fluka Analytical) and subsequently stored overnight at 100% relative humidity (RH) was brought into contact with a fluorinated Si (F-Si) surface and then withdrawn, all while monitoring the

deflection of the cantilever using an AFM (Dimension ICON, Bruker Corporation). All AFM experiments were performed at atmospheric pressure and room temperature (~21 ºC). F-Si surfaces were made by vapor-coating Si<100> wafers (Nova Electronic Materials, LLC) with heptadecafluoro-1,1,2,2-tetra(hydrodecyl)trichlorosilane (Gelest, Inc.) overnight in a desiccator. Similarly, Si<100> wafers were vapor-coated with hexamethyldisilazane (HMDS; Sigma-Aldrich) overnight in a desiccator to make the Me-Si substrates. For SiO_2 surfaces, unmodified Si<100> wafers were used directly without plasma cleaning to ensure that the surfaces would exhibit only partial wetting. Contact angle experiments were performed using the sessile-drop method in a contact-angle goniometer (FTA125, First Ten Angstroms). The droplets were measured 60 s after deposition, to ensure full relaxation; furthermore, adding volume to the droplets did not significantly change their measured contact angle.

To perform a deposition experiment, an AFM (NX-20, Park Systems AFM) was used to hold a tip array (type-M, NanoInk Inc.) in contact with F-Si for *t*. The tips were inked and stored at 100% RH in a similar manner to the patterning experiments. All patterning was carried out at ~100% RH. Subsequent AFM imaging (Dimension ICON, Bruker Corporation) was used to measure the topography of the residual material, which in all cases was present as sessile drops. The PEG-on-hydrophobic-surface system was chosen due to its widespread use in scanning probe-based molecular printing, where PEG functions as a matrix for transporting materials,[6, 8] a medium for performing chemical reactions[27-30], and displays low feature size variation during deposition[31].

RESULTS/DISCUSSION

In order to evaluate the role of the capillary meniscus in liquid-based DPN, AFM was used to record the force during the four stages of the writing process (Fig. 2a). This analysis (Fig. 2b) revealed that while approach curves (blue) were generally indistinguishable (steps i and ii), retraction curves (red) conveyed a great deal of information as they provide a picture of capillary rupture (steps iii and iv). In particular, by comparing two force-distance measurements recorded at different U (Fig. 2b, left) it is clear that there are two categorically different force profiles: when retracting quickly (U = 110 μm/s), the AFM jumps straight from the contact line to the free space line, while slow retraction (U = 0.03 μm/s) results in a force that smoothly decreases until it meets the free space line. This can be understood by considering that if the tip is being retracted sufficiently fast, the fluid has no time to rearrange in response to the applied force and thus the tip-sample force increases linearly until it reaches the maximum attractive force and suddenly releases. In contrast, if the probe is retracted slowly enough to allow fluid rearrangement, the fluid will flow within the meniscus in order to lower the area of the liquid on the surface, thereby reducing the net force from surface tension. This effect can be quantified by calculating the maximum attractive force F_{max} which, as predicted by this heuristic, monotonically increases with retraction speed (Fig. 2c). These data are well fit by a phenomenological three parameter first-order rational polynomial where the transition from the quasi-static regime to the dynamic regime is centered at $U = 6 \pm 2$ μm/s. Interestingly, using μ = 40 mP·s[32] and γ = 40 mN/m[33], we find that this speed corresponds to a critical capillary number $Ca = 6\times10^{-6}$, which is much smaller than the $\sim10^{-2}$ critical value commonly observed in bulk dewetting phenomena[16, 24, 25, 34]. However, this is consistent with what is seen in flow through porous materials[35] which is presumed to be due to the difference in length scales over which capillarity and viscosity are important. The similarity in phenomenology between these AFM-

based measurements and fluid flows in porous media presents an opportunity to gain insight into a more general class of fluid flow problems.

While U dominates F_{max}, the fluid is not expected to be static while the tip is in contact with the surface (step ii) and the time-dependent meniscus size may play a major role. For example, it has been hypothesized that the Laplace pressure of the meniscus will drive a flow between the tip and sample[10]. To explore this, we calculated the maximum height Z_{max} of the probe above the sample where there is still an attractive force (Fig. 2b, right). As t was increased from 0.1 s to 10 s (Fig. 2d) with U = 11 μm/s, Z_{max} increased monotonically in a manner that was well fit by a phenomenological power law with an exponent of 0.20 ± 0.02. This is remarkably similar to the 0.2 exponent observed in Tanner's law of droplet spreading, which could be due to the hydrophobic nature of the surface causing fluid flow to be dominated by rearrangement of fluid near the tip rather than flow from the tip to the surface. We note that varying the approach speed (step i) did not play a major role in the force-distance curves.

While the AFM-based experiments shed light on fluid behavior during capillary rupture, the material left behind on the surface can also provide insight into the fluid flow in this system (Fig. 3a). Furthermore, since depositing material is the goal of direct-write techniques such as DPN, the material deposited on a surface is of central importance in a lithographic context. In agreement with prior studies, V was shown to depend on t, with V approximately doubling over five orders of magnitude in t (Fig. 3b). When fit to a power law, we find $V \propto t^{0.15 \pm 0.02}$. Given the similarity between this power law and the rate of change of Z_{max} displayed in Fig. 2, we conclude that the contact area is not changing appreciably during dwell (step ii), but the drop is growing taller. This is in contrast with results from patterning on a more hydrophilic surface (500 nm thermal SiO_2 on Si<100>, Nova Electronic Materials, LLC; hereafter SiO_2) in which we find $V \propto$

$t^{0.46 \pm 0.06}$. This scaling is reminiscent of Lucas-Washburn capillary filling, which is consistent with a model of deposition that is dominated by capillary-driven fluid flow. Interestingly, Lucas-Washburn filling corresponds to axially-directed capillary filling in a tube while here the filling is directed radially on a surface. We believe this presents an intriguing opportunity for theoretical or computational study to understand the similarity between these phenomena. It is important to note that care had to be taken to prevent ink depletion during deposition of the features on SiO_2 (Fig. 3b); this was done by waiting for 60 s with the tips lifted between each programmed point.

To further illustrate the importance of surface energy, we compared the aspect ratios (ARs) of features printed by DPN on three surfaces (Fig. 3c), and correlated them with their bulk contact angle measurements. A difference was observed between the measured AR and the predicted AR from bulk contact angle measurements (red line in Fig. 3c), which suggests that small scale effects may be playing an important role. These effects potentially include disjoining pressure[26], elastocapillary phenomena[36], and line tension[37, 38]. If we assume that the dominant effect is line tension, we find a PEG-air-SiO_2 line tension of ~-0.002 μJ/m for features with a 130 nm radius of curvature and ~-0.06 μJ/m for features with a 5 μm radius of curvature, which are in agreement with previous observations[37]. The hypothesis that line tension is dominant in these experiments is also supported by the dependence of AR on size (Fig. 3d).

In order to explore the role of surface energy on the transition from quasi-static capillary rupture to dynamic capillary rupture, we performed a series of lithographic experiments on SiO_2 and F-Si, where U was varied from 0.1 to 100 μm/s (the full range of the instrument) with t = 1 s. For the polymer spots on SiO_2, V decreased with increasing U (Fig. 4a), in agreement with the conventional wisdom in DPN that slower processes result in larger features. In stark contrast, for patterning on hydrophobic surfaces, V became *larger* as U increased (Fig. 4b). These initially

surprising results can be explained in the context of liquid transfer during the separation of two surfaces[23, 24]. For a drop sandwiched between two flat surfaces, at sufficiently fast *U*, the drop's volume will be evenly split between the surfaces regardless of their surface energies. On the other hand, for slower *U*, the volumetric transfer ratio depends on the relative contact angles of the two surfaces with the lower contact angle surface retaining the majority of the material. These observations of transfer between two surfaces are in agreement with the trends observed here (Figs. 4a, b). In addition, the location of the transition in *U* (*i.e.* between 1 and 10 μm/s) is in agreement with the quasi-static-dynamic transition observed in AFM (Fig. 2c).

Understanding nanoscale fluid flows in molecular deposition allows one to make features that are considerably smaller than the maximum meniscus contact area (Fig. 5a). To demonstrate the potential of this approach for lithography, PEG was deposited onto F-Si using a 1-D probe array with $U = 0.1$ μm/s and $t = 1$ s. AFM topographical imaging revealed that PEG features as small as 14 nm in diameter were printed (Fig. 5b); notably, this corresponds to ~40 molecules of PEG2000. To compare the maximum size of the meniscus to the size of the deposited feature, we used AFM phase imaging which revealed a >250 nm diameter region encompassing each polymer feature (Fig. 5c). Due to the lack of a topographical feature with a corresponding size, we attribute this phase contrast to changes in the surface chemistry due to exposure to the polymer/water meniscus. Therefore, these transferred polymer features were approximately an order of magnitude smaller in diameter than the meniscus. Interestingly, such halos were not present around features written on SiO_2, in agreement with our hypothesis that slowly retracting the tip from hydrophobic surfaces allows for the contact area to shrink prior to capillary rupture.

In conclusion, we have elucidated the nanoscale fluid phenomena that play major roles in DPN of liquids. In particular, we found that the dynamics of transfer and capillary rupture are

highly dependent on surface energy, a fact which may be partly responsible for the apparently contradictory data in the literature related to the dynamics of liquid transfer. From a lithographic perspective, the concepts outlined here illustrate that patterning on highly hydrophobic surfaces is advantageous because (a) the deposited features are small compared to those deposited on hydrophilic surfaces and thus (b) there is less ink depletion; furthermore, from an imaging perspective, (c) the high aspect ratios on such surfaces of polymeric features make them easy to visualize. These results may be useful for deposition of the wide array of liquid inks that have been studied including polymers[19, 31], phospholipids[39, 40], and nonvolatile fluids[6, 28, 41]. Finally, these results highlight that not only is DPN a rich fluidic system with many nuances yet to be understood, but also that lessons garnered from these types of study could provide insights into more fundamental questions, *e.g.* the nature of line tension, capillarity on the nanoscale, or elastocapillary phenomena.

REFERENCES

1. R. B. Schoch, J. Han and P. Renaud, *Rev. Mod. Phys.*, 2008, **80**, 839-883.
2. R. D. Piner, J. Zhu, F. Xu, S. H. Hong and C. A. Mirkin, *Science*, 1999, **283**, 661-663.
3. D. S. Ginger, H. Zhang and C. A. Mirkin, *Angew. Chem. Int. Edit.*, 2004, **43**, 30-45.
4. K. Salaita, Y. H. Wang and C. A. Mirkin, *Nature Nanotech.*, 2007, **2**, 145-155.
5. K. A. Brown, D. J. Eichelsdoerfer, X. Liao, S. He and C. A. Mirkin, *Front. Phys. China*, 2014, **9**, 385-397.
6. L. Huang, A. B. Braunschweig, W. Shim, L. Qin, J. K. Lim, S. J. Hurst, F. Huo, C. Xue, J.-W. Jang and C. A. Mirkin, *Small*, 2010, **6**, 1077-1081.
7. R. F. Jonathan, S. Suhas, H. E. Randy and P. K. William, *Nanotechnology*, 2012, **23**, 215301.
8. J. A. Chai, F. W. Huo, Z. J. Zheng, L. R. Giam, W. Shim and C. A. Mirkin, *Proc. Natl. Acad. Sci. U. S. A.*, 2010, **107**, 20202-20206.
9. G. Liu, Y. Zhou, R. S. Banga, R. Boya, K. A. Brown, A. J. Chipre, S. T. Nguyen and C. A. Mirkin, *Chem. Sci.*, 2013, **4**, 2093-2099.
10. C. D. O'Connell, M. J. Higgins, D. Marusic, S. E. Moulton and G. G. Wallace, *Langmuir*, 2014, **30**, 2712-2721.
11. A. Lutfurakhmanov, G. K. Loken, D. L. Schulz and I. S. Akhatov, *Appl. Phys. Lett.*, 2010, **97**, 124107.
12. J. Crassous, E. Charlaix and J.-L. Loubet, *Phys. Rev. Lett.*, 1997, **78**, 2425-2428.

13. J. Jang, G. C. Schatz and M. A. Ratner, *Phys. Rev. Lett.*, 2003, **90**, 156104.
14. H. Kim, L. C. Saha, J. K. Saha and J. Jang, *Scanning*, 2010, **32**, 2-8.
15. H. Kim, B. Smit and J. Jang, *J. Phys. Chem. C*, 2012, **116**, 21923-21931.
16. J. Bowen, D. Cheneler, J. W. Andrews, A. R. Avery, Z. Zhang, M. C. L. Ward and M. J. Adams, *Langmuir*, 2011, **27**, 11489-11500.
17. D. L. Malotky and M. K. Chaudhury, *Langmuir*, 2001, **17**, 7823-7829.
18. J. Y. Jang, S. H. Hong, G. C. Schatz and M. A. Ratner, *J. Chem. Phys.*, 2001, **115**, 2721-2729.
19. A. Hernandez-Santana, E. Irvine, K. Faulds and D. Graham, *Chem. Sci.*, 2011, **2**, 211-215.
20. R. McKendry, W. T. S. Huck, B. Weeks, M. Fiorini, C. Abell and T. Rayment, *Nano Lett.*, 2002, **2**, 713-716.
21. L. M. Demers, D. S. Ginger, S.-J. Park, Z. Li, S.-W. Chung and C. A. Mirkin, *Science*, 2002, **296**, 1836-1838.
22. J. H. Lim and C. A. Mirkin, *Adv. Mater.*, 2002, **14**, 1474-1477.
23. A. V. Chadov and E. D. Yakhnin, *Colloid J. USSR*, 1979, **41**, 817-820.
24. E. D. Yakhnin and A. V. Chadov, *Colloid J. USSR*, 1983, **45**, 1183-1188.
25. P. Darabi, T. Li, K. Pougatch, M. Salcudean and D. Grecov, *Chem. Eng. Sci.*, 2010, **65**, 4472-4483.
26. J. W. van Honschoten, N. Brunets and N. R. Tas, *Chem. Soc. Rev.*, 2010, **39**, 1096-1114.
27. S. Bian, A. M. Scott, Y. Cao, Y. Liang, S. Osuna, K. N. Houk and A. B. Braunschweig, *J. Amer. Chem. Soc.*, 2013, **125**, 9240-9243**.**
28. S. Bian, K. B. Schesing and A. B. Braunschweig, *Chem. Commun.*, 2012, **48**, 4995-4997.
29. S. Bian, J. He, K. B. Schesing and A. B. Braunschweig, *Small*, 2012, **8**, 2000-2005.
30. G. Liu, D. J. Eichelsdoerfer, B. Rasin, Y. Zhou, K. A. Brown, X. Liao and C. A. Mirkin, *Proc. Natl. Acad. Sci. U. S. A.*, 2013, **110**, 887-891.
31. D. J. Eichelsdoerfer, K. A. Brown, M. X. Wang and C. A. Mirkin, *J. Phys. Chem. B*, 2013, **117**, 16363-16368.
32. T. Murugesan and M. Perumalsamy, *J. Chem. Eng. Data*, 2005, **50**, 1290-1293.
33. G. Korosi and E. S. Kovats, *J. Chem. Eng. Data*, 1981, **26**, 323-332.
34. J. H. Snoeijer, G. Delon, M. Fermigier and B. Andreotti, *Phys. Rev. Lett.*, 2006, **96**, 174504.
35. R. T. Armstrong, A. Georgiadis, H. Ott, D. Klemin and S. Berg, *Geophys. Res. Lett.*, 2014, **41**, 55-60.
36. D. L. Henann and K. Bertoldi, *Soft Matter*, 2014, **10**, 709-717.
37. R. David and A. W. Neumann, *Langmuir*, 2007, **23**, 11999-12002.
38. J. H. Weijs, A. Marchand, B. Andreotti, D. Lohse and J. H. Snoeijer, *Phys. Fluids* 2011, **23**, 022001-022011.
39. S. Lenhert, F. Brinkmann, T. Laue, S. Walheim, C. Vannahme, S. Klinkhammer, M. Xu, S. Sekula, T. Mappes, T. Schimmel and H. Fuchs, *Nature Nanotech.*, 2010, **5**, 275-279.
40. S. Lenhert, P. Sun, Y. H. Wang, H. Fuchs and C. A. Mirkin, *Small*, 2007, **3**, 71-75.
41. A. J. Senesi, D. I. Rozkiewicz, D. N. Reinhoudt and C. A. Mirkin, *ACS Nano*, 2009, **3**, 2394-2402.

ACKNOWLEDGMENTS

The authors would like to thank Prof. Franz Geiger for use of his contact-angle goniometer. C.A.M. acknowledges the U.S. Air Force Office of Scientific Research (AFOSR, Awards FA9550-12-1-0280 and FA9550-12-1-0141), and the National Science Foundation (NSF, Award DBI-1152139) for support of this research. D.J.E. acknowledges the Department of Defense and AFOSR for a National Defense Science and Engineering Graduate (NDSEG) Fellowship, 32 CFR 168a. K.A.B. gratefully acknowledges support from Northwestern University's International Institute for Nanotechnology.

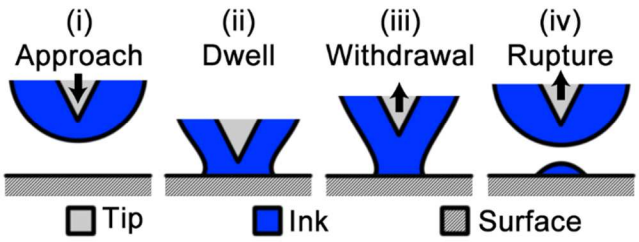

Figure 1. Schematic showing the four stages of material transfer from a fluid-coated atomic force microscopy (AFM) probe to a surface.

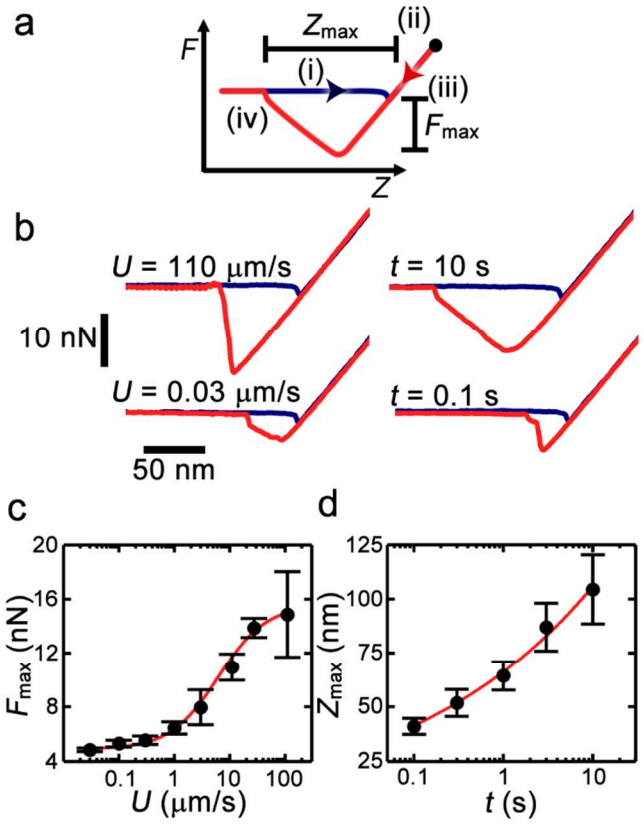

Figure 2. AFM force-distance analysis of material deposition. (a) Schematic showing how the four stages of deposition correspond to the tip-sample distance Z and measured force F. (b) Four example force-distance curves showcasing the range of phenomena observed at different retraction speeds U and dwell times t. (left) Data taken with t = 1 s. (right) Data taken with U = 11 μm/s. (c) Maximum force (F_{max}) observed at different U. Each point corresponds to nine measurements with error bars given by their standard deviation. The red line is a phenomenological fit to a first order rational polynomial. (d) Meniscus height (Z_{max}) observed at different t. Each point corresponds to nine measurements with error bars given by their standard deviation. The red line represents a phenomenological fit to a power law with no offset.

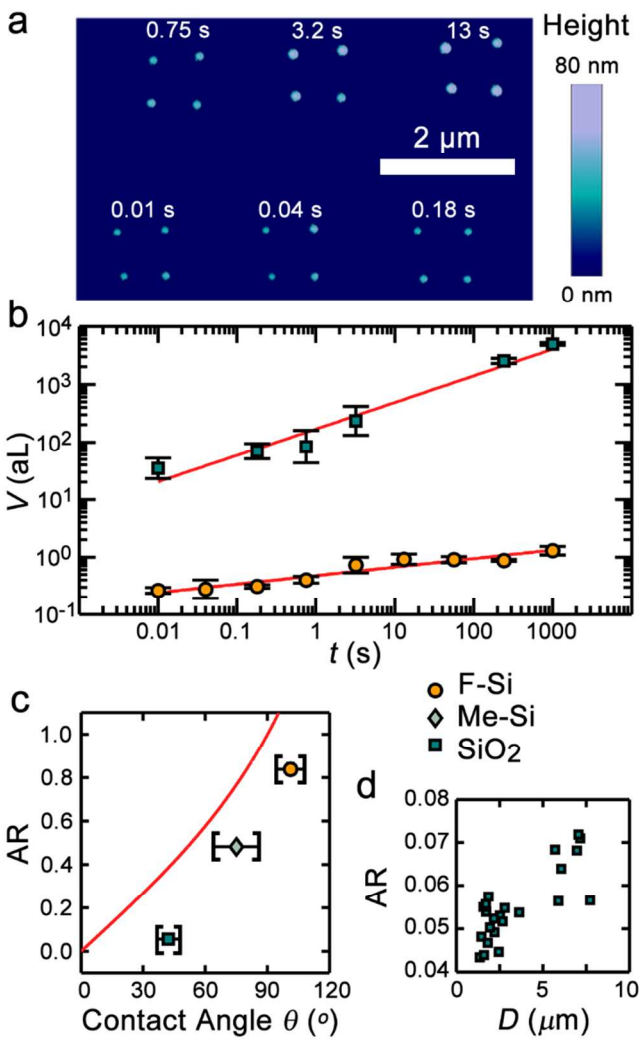

Figure 3. Imaging the residual material following deposition. (a) AFM topographic image of dot features written on fluorinated silicon (F-Si) with U = 100 µm/s and t as shown in the image. (b) Volume V of features written at different t on F-Si and oxide-coated silicon (SiO_2). Each point is the average of four features with the error bars corresponding to the standard deviation. Lines are fits to power laws with no offsets. (c) Aspect ratio (AR; defined as the ratio of feature height over feature radius) of features on F-Si, SiO_2, and hexamethyldisilazane-coated Si (Me-Si). Here, feature height and radius were determined by AFM to be the maximum height of a given feature and half the width of the base of the feature, respectively. The horizontal brackets correspond to the range of contact angles observed for ethylene glycol and water; these are assumed to

encompass the surface energy of the feature, which is a mixture of water and poly(ethylene glycol). Vertical error bars are smaller than the point size. The red line corresponds to the AR of a spherical cut with a given contact angle. (d) AR of features with different diameters *D* written on silica.

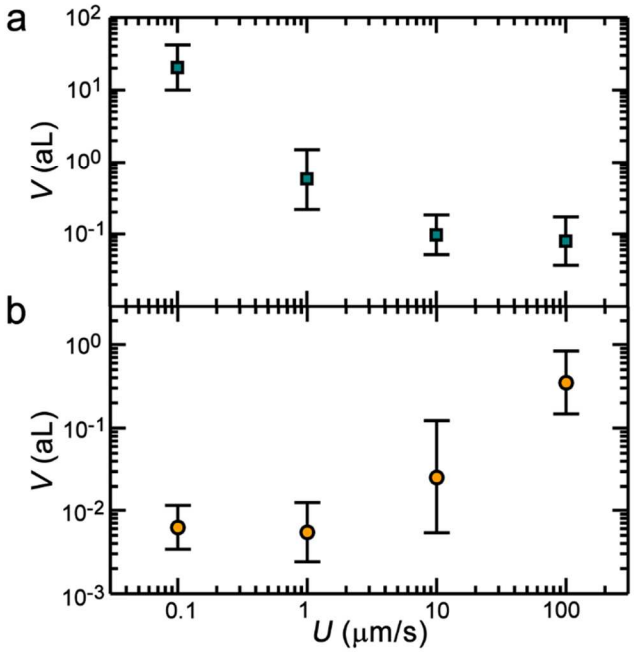

Figure 4. *V* of features written on SiO_2 (a) and F-Si (b) at different *U*. Features in (a) correspond to the mean of eight points taken over two cycles of decreasing *U* with the error bars displaying their standard deviation. Features in (b) correspond to 32 points taken over two cycles of *U* with the error bars displaying their standard deviation. In all experiments, $t = 1$ s.

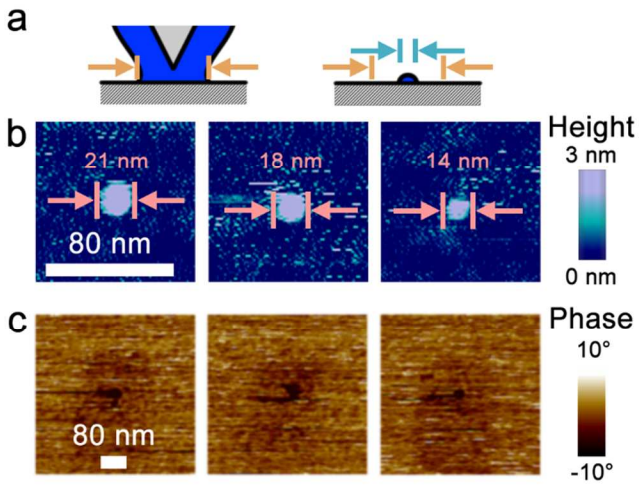

Figure 5. Comparison of meniscus size and transferred polymer feature. (a) Schematic showing the maximum meniscus profile during step (ii) as compared to the much smaller size of the transferred feature after capillary rupture (step iv). (c) AFM topographical imaging of three features written with U = 0.1 µm/s and t = 1 s. The mean diameter of all features written at this condition was found to be 30 ± 10 nm, not accounting for a ~3 nm radius of curvature of the AFM probe. (c) AFM phase imaging of the region surrounding each feature shown in (b). The black spot in the center is due to the feature and the dark halo is a reflection of the maximum meniscus size.